Wind and Structures, *Vol. 20, No. 3 (2015) 449-468*
DOI: http://dx.doi.org/10.12989/was.2015.20.3.449

Influence of ventilation rate on the aerodynamic interference between two extra-large indirect dry cooling towers by CFD

S.T. Ke[*1], J. Liang[1a], L. Zhao[2b] and Y.J. Ge[2c]

[1]*Department of Civil Engineering, Nanjing University of Aeronautics and Astronautics, 29 Yudao Road, Nanjing 210016, China*
[2]*State Key Laboratory for Disaster Reduction in Civil Engineering, Tongji University, 1239 Siping Road, Shanghai 200092, China*

(Received August 3, 2014, Revised January 24, 2015, Accepted January 27, 2015)

Abstract. Current wind-resistance designs of large-scale indirect dry cooling towers (IDCTs) exclude an important factor: the influence of the ventilation rate for radiator shutter on wind loads on the outer surfaces of the tower shell. More seemingly overlooked aspects are the effects of various ventilation rates on the wind pressure distribution on the tower surfaces of two IDCTs, and the feature of the flow field around them. In order to investigate the effects of the radiator shutter ventilation rates on the aerodynamic interference between IDCTs, this paper established the numerical wind tunnel model based on the Computational Fluid Dynamic (CFD) technology, and analyzed the influences of various radiator shutter ventilation rates on the aerodynamic loads acting upon a single and two extra-large IDCTs during building, installation, and operation stages. Through the comparison with the results of physical wind tunnel test and different design codes, the results indicated that: the influence of the ventilation rate on the flow field and shape coefficients on the outer surface of a single IDCT is weak, and the curve of mean shape coefficients is close to the reference curve provided by the current design code. In a two-tower combination, the ventilation rate significantly affects the downwind surface of the front tower and the upwind surface of the back tower, and the larger positive pressure shifts down along the upwind surface of the back tower as the ventilation rate increases. The ventilation rate significantly influences the drag force coefficient of the back tower in a two-tower combination, the drag force coefficient increases with the ventilation rate and reaches the maximum in a building status of full ventilation, and the maximum drag coefficient is 11% greater than that with complete closure.

Keywords: extra-large indirect dry cooling towers; wind loads; aerodynamic interference; CFD; wind tunnel test; ventilation rate

1. Introduction

As important buildings in fossil-fuel power plants and thermal power plants in Northwest

∗Corresponding author, Associate Professor, E-mail: keshitang@nuaa.edu.cn
[a] Postgraduate, E-mail: liangjun@nuaa.edu.cn
[b] Professor, E-mail: zhaolin@tongji.edu.cn
[c] Professor, E-mail: yaojunge@tongji.edu.cn

http://www.techno-press.org/?journal=was&subpage=8 ISSN: 1226-6116 (Print), 1598-6225 (Online)

China, extra-large indirect dry cooling towers (IDCTs) are typical wind-sensitive structures with low natural frequencies and complex 3-D vibrational modes (Armitt 1980, Jeong 2004, Noh and Lee 2013). The greatest differences between an extra-large IDCT and a natural draft hyperbolic cooling tower are that vertical radiator shutters and the broadening platforms are equipped around the bottom peripheral of an IDCT, the oblique support columns at the bottom inlets of the IDCT are higher, and the IDCT shell appears to be shorter and stouter. Figs. 1(a) and 1(b) show the overall configuration of an IDCT and the shutters installed around the radiator.

Since the wind-induced failure of the cooling tower group at Ferry Bridge in England in 1965 (Niemann and Kopper 1998), many scholars (Viladka *et al*. 2006, Harte and Wittek 2009, Ke *et al*. 2012, Zhang *et al*. 2014) have investigated the interference of wind loads on towers in cooling tower groups and the wind pressures characteristics on both inner and outer surfaces of tower shells. Orlando (2001) studied the aerodynamic interference between two adjacent cooling towers and summarized the distributions of the aerodynamic loads and wind-induced responses of the cooling towers with different distances between towers and various wind azimuths. Goodarzi (2010) analyzed the distribution characteristics of lateral aerodynamic forces on dry cooling towers and proposed a method to calculate the wind-induced response of a dry cooling tower under lateral winds, then suggested several measures to reduce the wind-induced effects. Goudarzi *et al*. (2008) proposed a fitting formula and coherence function of spectral characteristics of external wind pressure by comparing measured wind pressure to simulated wind pressure of large cooling towers in an Iranian power plant. Sun and Gu (1995) and Bartoli *et al*. (1997) studied interference effects of surrounding buildings on wind loads of group towers through pressure measurement in rigid body wind tunnel tests. Busch, *et al*. (2002) calculated wind-induced responses of large cooling towers and the influences of damping ratios, and other surrounding interferences were also analyzed based on rigid body pressure measurements and random vibration theory. Zhao and Ge (2010) investigated the correlation of pulsing wind pressures on the surfaces of extra-large cooling towers by means of wind tunnel tests, and summarized the magnification coefficients and drag coefficients of cooling tower groups with different tower types and distances. Results of the above work provide scientific foundations for designing large cooling towers, however, they are obtained for natural draft hyperbolic cooling towers and cannot be used directly for the wind-resistant design of indirect dry cooling towers due to the influences of the broad platforms and radiator shutters. So far, there have been very few studies on the influences of the broad platforms and radiator shutters of IDCTs on wind pressure distribution on the surfaces or the aerodynamic interference between adjacent towers. As a result, the study of the aerodynamic effects of the broad platforms and radiator shutters of IDCTs reported in this paper is of importance in an engineering aspect.

In this paper, the research object was an extra-large hyperbolic reinforced-concrete IDCT equipped in a 2×350MW indirect dry cooling assembly project in Northwest China. The parameters of this cooling tower are listed in Table 1.

The ventilation rate of radiator shutters varied indifferent stages of the building and operation of the IDCT. According to the characteristics of building and operation, the ventilation rates were determined as follows:

1)During the building of the IDCT, since the oblique columns at the inlets were the only obstacles for the wind, the shutters were assumed to be fully ventilating, i.e., the ventilation rate was 100%.

2)In the operational stage, when wind speed was below the design value, shutters on the peripheral of the radiator were open to a uniform degree. The shutters exerted different drags on

the incoming wind as the shutter degrees changed. Two working conditions with comprehensive ventilation rates of 30% and 15% were considered.

3)Also in the operational stage, when wind speed was above the design value in anti-freezing working conditions, the shutters were completely closed, meaning the ventilation rate was 0%.

(a) Global configuration (b) Local structure of radiator shutters

Fig. 1 Global and local views of an extra-large IDCT

Table 1 Size parameters of primary parts and structural schematic of the IDCT

Part	Size	Schematic
Tower height	180 m	
Throat altitude	158.4 m	
Inlet altitude	27.5 m	
Top radius	51.74 m	
Bottom radius	83.7 m	
Throat radius	51.0 m	
Thickness	0.35-2.4 m	
Rect. cross sections of columns	1.2 m×2 m	
Foundation (width×height)	12 m× 2 m	

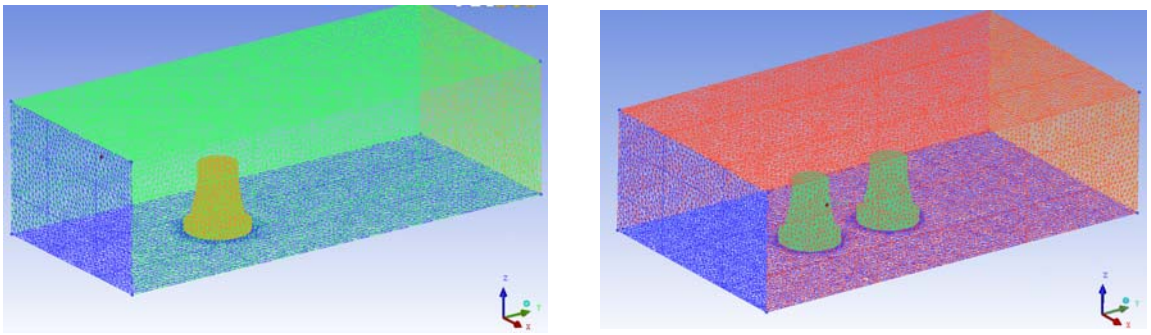

(a) Single tower model (b) Two-tower model

Fig. 2 Schematics of computational domains

In this paper, the flow fields in four working conditions with four different ventilation rates (100%, 30%, 15% and 0%) in the building and operational stages were numerically simulated by means of CFD and wind tunnel tests. The distribution of pressure coefficients on a single tower and on two-tower combinations were analyzed and compared with the curve of pressure coefficient distributions provided by the current design codes for verification. At the same time, the curves of the flow field and global drag coefficients of IDCTs with different ventilation rates varying with the wind azimuth were given. Based on these results, the rules and mechanisms of the influence of the broad platform and the radiator shutter ventilation rates on aerodynamic loads on a single IDCT and double IDCTs were obtained.

2. CFD models and parameters

2.1 CFD models

CFD numerical simulations in this paper made use of a RNG k-ε turbulence model (Schmidt and Thiele 2002), which took turbulent eddies into account based on the standard k-ε model proposed by Launder and improves the accuracy of the simulations with high Reynolds numbers. Since it was especially suitable for numerical analysis of problems such as flow around giant buildings and boundary layer flow, the RNG k-ε turbulence model was chosen for flow simulations of extra-large cooling towers. The computational domain size was 1246 m×1066 m×360 m. X was lateral to the wind direction, Y was parallel to wind direction, and Z was the altitude direction. In order to obtain better agreement between experimental and numerical results, boundary conditions adopted in the numerical simulations should be the same as those in the experiments, especially for inflow boundary conditions. Boundary conditions at the inlet were set up by coding a user defined function (UDF), the velocity profile of atmospheric boundary layer was simulated according to the results in wind tunnel test. The maximum blocking probability was less than 5%. The computational domains for different models are shown in Fig. 2.

The variables in the RNG *k-ε* turbulence model (turbulent kinetic energy *k*, turbulent dissipation rate ε and turbulent frequency *w*) were given. The integral size was determined by the actual size. The wind field was simulated by an exponential velocity profile, in which the

distribution of the wind velocity with altitude was given by $V_z=V_{ref}(z/10)^{\alpha}$, where α=0.15, V_z was the wind velocity at the altitude z, the reference altitude was chosen as Z_{ref}=10 m. The reference wind velocity was set to be the maximum mean wind velocity of 10min at 10m for a wind that has the probability of occurring once in 50 years. Pressure at the outlet was specified for the boundary condition. Non-slip conditions were satisfied for all walls. The coupling between velocity and pressure was solved by the SIMPLEC method. Air was modeled as an incompressible perfect gas. Discretization of the convective term was implemented by the relatively more accurate second order upwind format with a tolerance for convergence of 10^{-4}. The numerical time step for the RNG *k*-ε turbulence model was 2×10-3 s, 2000 steps were iterated to obtain the time-averaged results.

The control of mesh quality is difficult for structures with a large amount of fine parts such as IDCTs. To improve the computational efficiency without sacrificing accuracy, a mixed meshing approach was employed in this paper, which refined the mesh near the radiator. The least discretization size was as small as 0.2 m at the connections between the columns and the tower shell, while the characteristic size of elements was as large as 2 m at the boundary of the flow domain where the mesh was the sparsest. The number of elements reached 5.2 million for meshes. The meshes for different models are shown in Fig. 3.

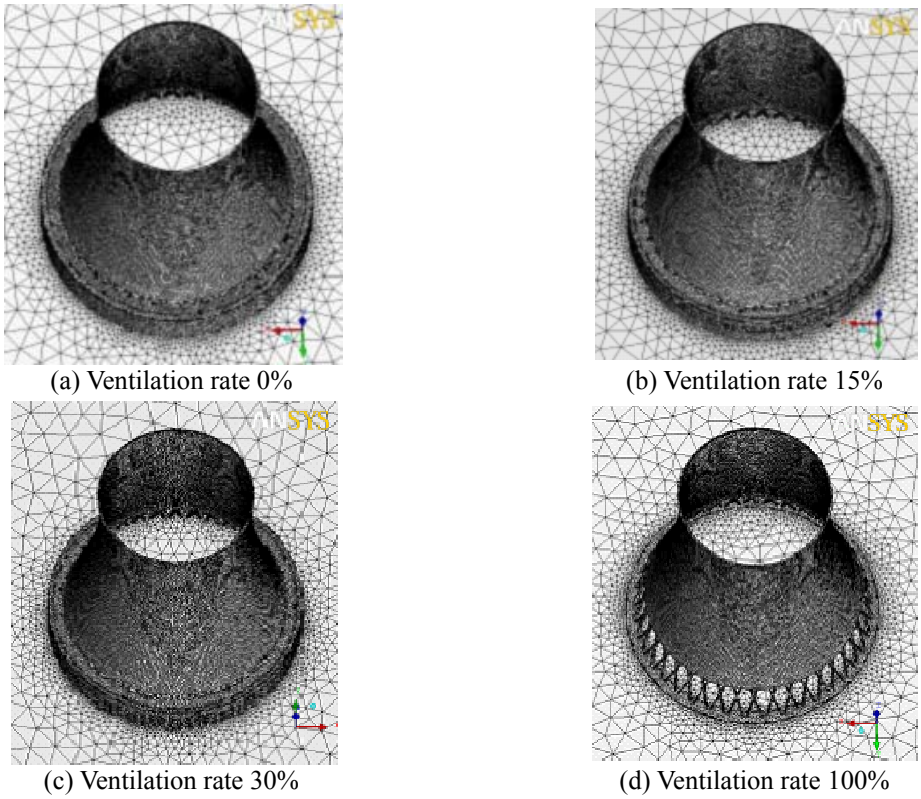

(a) Ventilation rate 0% (b) Ventilation rate 15%

(c) Ventilation rate 30% (d) Ventilation rate 100%

Fig. 3 Schematics of meshes for the different models

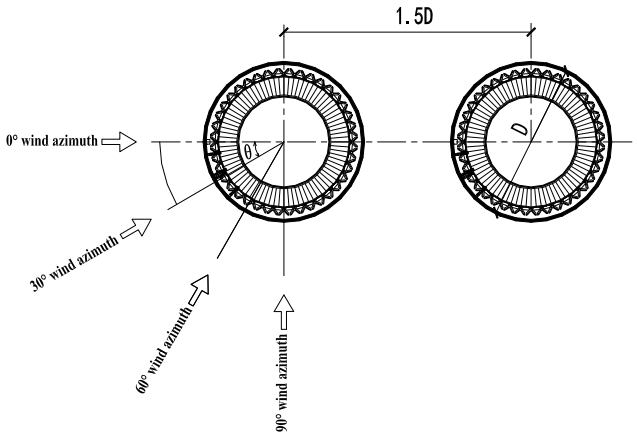

Fig. 4 Schematic of the incoming wind azimuth in a two-tower combination

2.2 Definitions of parameters

Wind pressure on the structural surface is defined by the non-dimensional wind pressure coefficient

$$C_{pi,\theta} = \frac{P_{i,\theta} - \overline{P}_s}{\overline{P}_{t,h} - \overline{P}_s} = \frac{P_{i,\theta} - \overline{P}_s}{0.5\rho\overline{V}_h^2} \tag{1}$$

Where $C_{pi,\theta}$ is the wind pressure coefficient at point i under wind azimuth θ, $P_{i,\theta}$ is the pressure at point i under wind azimuth θ, $\overline{P}_s$ is the mean static pressure at the reference point, $\overline{P}_{t,h}$ is the total pressure at the reference altitude h, ρ is the density of air, $\overline{V}_h$ is the mean wind velocity at the reference altitude h. For convenience, the altitude of the reference point was chosen as h=10 m.

Shape coefficient is transformed from nodal pressure coefficient

$$\mu_{i,\theta} = \frac{\overline{C}_{pi,\theta}}{\left(Z_i/h\right)^{2\alpha}} \tag{2}$$

Where $\mu_{i,\theta}$ is the shape coefficient at point i, Z_i is the altitude of the point i, α is the ground roughness exponent which was set to be 0.15 according to Type B in the code.

Global drag coefficient is calculated as

$$C_D = \left(\sum_{i=1}^{N} C_{pi,\theta} A_i \cos\theta_i\right) / A_T \tag{3}$$

Where C_D is the global drag coefficient of the structure, $C_{pi,\theta}$ is the wind pressure coefficient at point i under wind azimuth θ, A_i is the area covered by pressure at point i, A_T is the area of the overall structure projected to the wind direction.

2.3 Definition of wind azimuth

The distance between towers in a two-tower interference model is 1.5D (D is the bottom diameter of an IDCT) according to the German code of design for IDCTs (VGB-Guideline, 2005). The horizontal direction in the plane connecting the axes of the two towers is defined as 0° wind azimuth. A nonzero wind azimuth is obtained by a counterclockwise rotation from 0° wind azimuth, which is indicated in Fig. 4.

3. Wind tunnel experiment

In order to verify the numerical evaluation of a single IDCT by CFD, the test was carried out in the NH-2 atmospheric boundary wind tunnel at Nanjing University of Aeronautics and Astronautics to obtain the pressure distribution on IDCTs with different ventilation rates. The wind tunnel section is 5.0 m wide and 4.2 m high. The geometrical scale used was 1:200, and a total of 432 measuring taps were arranged in the IDCT. Fluctuating wind pressures at 330 Hz were simultaneously measured at the 432 measuring taps on a rigid model of the IDCT. Pressure taps were connected with a measurement system made of PVC tubing. Signals were modified using the transfer function of the tubing systems to avoid distortion of the dynamic pressures. Fig. 5 presents the photograph of the rigid model and pressure taps layout for a single IDCT.

The wind field of terrain category B, in accordance with the Chinese Code (GB5009-2012 2012), was simulated with a standard spire-roughness arrangement on the wind tunnel floor. The exponent of the mean wind speed profile for terrain category B was 0.15. The reference wind speed height is 0.9 m in wind tunnel. The power function of fluctuant wind speed at the reference height in the wind tunnel is shown in Fig. 6.

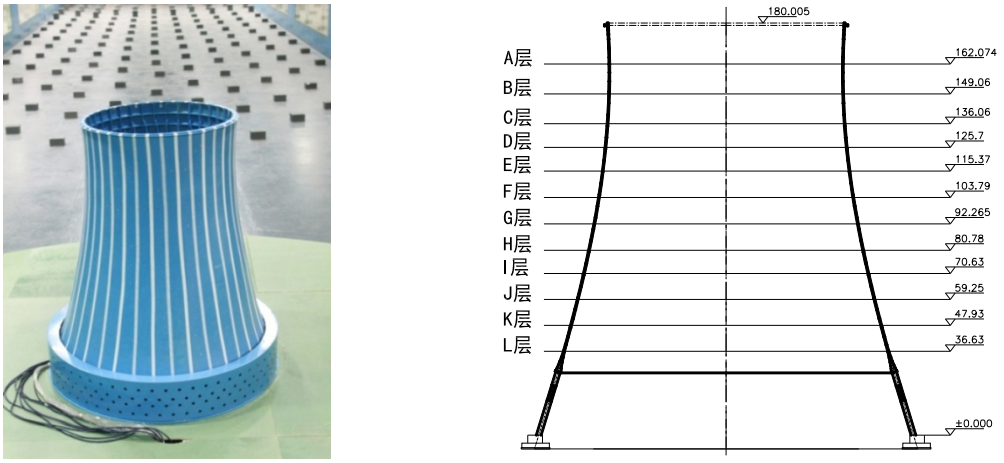

(a) Rigid model (b) pressure taps layout

Fig. 5 Rigid model and pressure taps layout of a single IDCT for wind tunnel test

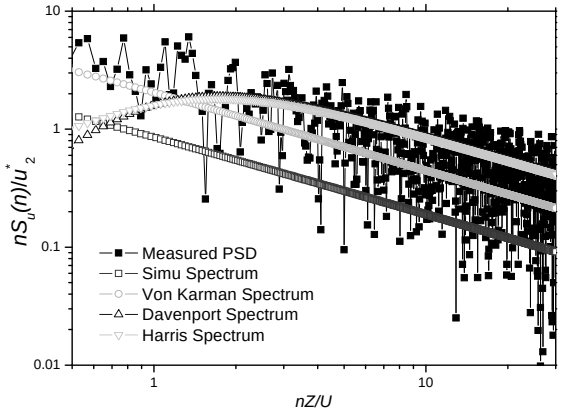

Fig. 6 Power spectral function of along wind component in NH-2 wind tunnel

Flow-induced forces on curved bodies, like cooling towers, depend strongly upon Reynolds number Re (Re = UD/υ, where U is the mean velocity of the undisturbed flow, D is the tower diameter, υ is the kinematic viscosity of air) and surface roughness. Re in the wind should be the same as in full scale, however, adjusting velocity is impossible since the velocity in the tunnel should be 200 times the full-scale one according to the Re effect. Usually, the difference of the Reynolds number between test and prototype can be overcome with modification of the model surface roughness for aero-elastic model of super-large cooling towers (Zhao and Ge 2010, Goudarzi *et al*. 2008).The simulation targets about surface flow parameters, such as Maximum and Minimum pressure values and its angles, zero pressure angle, separation angle, Strouhal number, etc..With the aid of sticking paper belts along vertical direction and adjusting incoming wind velocity, the actual aerodynamic characteristics of archetype cooling towers are successfully re-illustrated in the reduced-scale model with lower Reynolds number. More wind tunnel test outlines of cooling towers can be found in the literature (Ke *et al*. 2012, 2013).

4. Results and discussions

4.1 Numerical calibration

The present numerical calibration is considered for a single IDCT under 0° wind azimuth. The numerical results obtained from the RNG k-ε turbulence model and mixed meshing approach are computed under the same inflow boundary conditions as those simulated in the wind tunnel test mentioned in section 3. The drag force coefficients, their root mean square (rms) values and separation angles for IDCTs with different ventilation rates are compared with the available experiment data, as shown in Table 2.

Comparing the results of the four models listed in Table 1, it is obvious that the k-ε turbulence model is helpful to improve the prediction of drag force coefficients CD of different calculating models to a satisfactory level with error < 5%. The predicted rms coefficient CD is also very close to the experimental result and the maximum error is less than 10% under 0% ventilation rate. For

different calculating models, the separation angle mainly occurs at between 115° and 120°.

To further checking the validity of using CFD to simulate the pressure distribution on the surfaces of extra-large IDCTs and to reveal the influence of ventilation rate to the pressure distribution on the surface of a single IDCT, Fig. 7 shows the distribution curve of the circumferential shape coefficients of a single IDCT at throat altitude under four different ventilation rates. Figures8 and 9 demonstrate the distribution curves of the circumferential shape coefficients of each tower in the two-tower combination at the throat cross section under four different ventilation rates. Due to symmetry of the structure, only the shape coefficients in the circumferential range of 0-180°angles are plotted and compared to the curves of ribbed cooling towers and cooling tower without ribs of Chinese norm and to the K1.6 curve of German norm (VGB-Guideline, 2005). It is necessary to note that the curves of shape coefficient distribution given by norms were obtained from results of on-site measurements of natural draft cooling towers, in which the influence of radiator shutter ventilation rate was excluded.

Table 2 Comparison of the results from different calculating models and experiments for a single IDCT

Calculating model	Calculating case	C_D (dimensionless)	rms_{CD} (dimensionless)	Separation angle (°)
0% ventilation rate	CFD	0.362	0.016	115
	Wind tunnel test	0.369	0.018	120
15% ventilation rate	CFD	0.377	0.021	120
	Wind tunnel test	0.381	0.022	120
30% ventilation rate	CFD	0.408	0.024	115
	Wind tunnel test	0.402	0.025	115
100% ventilation rate	CFD	0.419	0.030	115
	Wind tunnel test	0.412	0.029	115

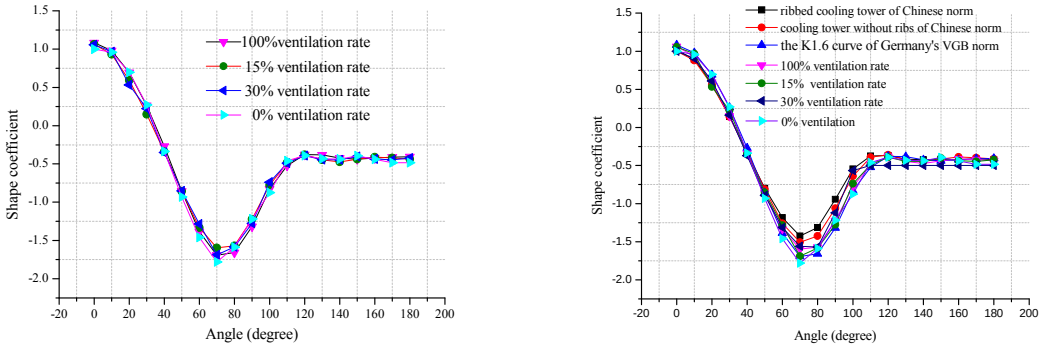

(a) Curves under different ventilation rates

(b) Comparison of curves and curves given by norms

Fig. 7 The shape coefficients of a single tower at the throat cross section under different ventilation rates

The comparison of the curves indicate that the curves of shape coefficient distribution of a single IDCT under different ventilation rates were close to the curves provided by norms, which verifies the validity of adopting CFD to simulate the pressure distribution on surfaces of extra-large IDCTs. For a two-tower combination, the curves of shape coefficient distribution of both towers deviated significantly from the curves provided by norms, and the deviations of the curves of the back tower were greater owing to the eclipsing effect of the front tower onto the back tower.

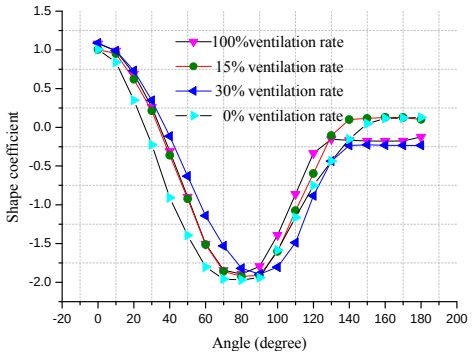

(a) Curves under different ventilation rates

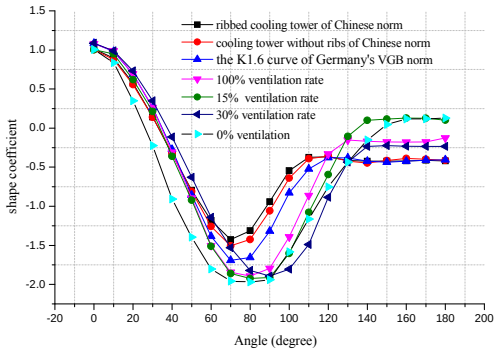

(b) Comparison of curves s and curves given by norms

Fig. 8 The shape coefficients of the front tower in a two-tower combination at the throat cross section under different ventilation rates

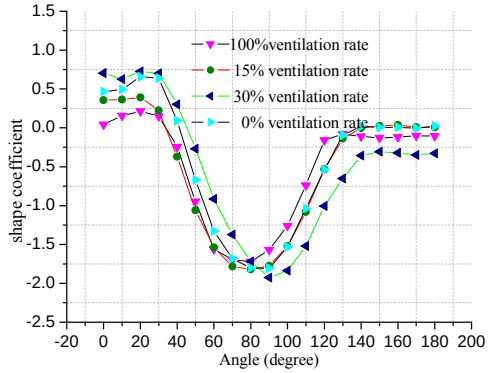

(a) Curves under different ventilation rates

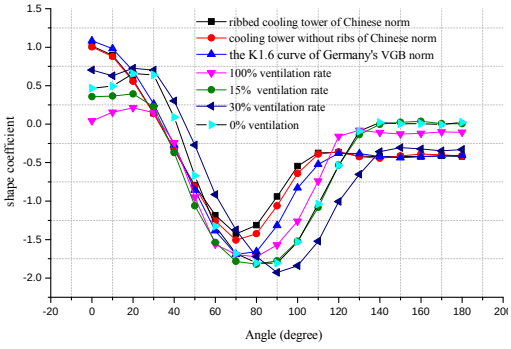

(b) Comparison of curves and curves given by norms

Fig. 9 The shape coefficients of the back tower in a two-tower combination at the throat cross section under different ventilation rates

4.2 Wind pressure distribution

Figs. 10 and 11 demonstrate the contours of pressure coefficients distribution on the outer and inner surfaces of a single extra-large IDCT with different ventilation rates. It can be seen that the pressure coefficients distributions on the outer surface with different ventilation rates tend to be consistent, and the pressure is mainly positive on the upwind surface and negative on both the downwind and lateral surfaces. Additionally, the ventilation rate influences the internal pressure of the IDCT, which decreases as the ventilation rate increases. This means that the influence of the ventilation rate on the mean pressure coefficients on the outer surface of a single IDCT is small, however, the influence of the ventilation rate on mean pressure coefficients on inner surface should be considered.

Fig. 12 shows the contours of pressure coefficients of a two-tower combination with different ventilation rates in 0° wind azimuth. From these contours, it can be seen that the distribution of pressure coefficients on the upwind surface of the front tower is consistent with the result of a single tower and the distributions of pressure coefficient on this surface with different ventilation rates are close to each other. The ventilation rate significantly affects the pressure coefficients on the upwind surface of the back tower and the downwind surface of the front tower. The effect of the ventilation rates of the pressure coefficients on the downwind surface of the back tower and lateral surfaces on both sides of both towers is relatively small. Due to the eclipsing effect of the front tower, the pressure coefficients on the upwind surface of the back tower are less than that on the front tower. As the ventilation rates increases, the pressure coefficient on the upwind surface of the back tower transforms from a symmetrical distribution to an asymmetrical distribution and the region where positive pressure reaches extreme values shifts gradually from the upper to the lower parts of the tower shell.

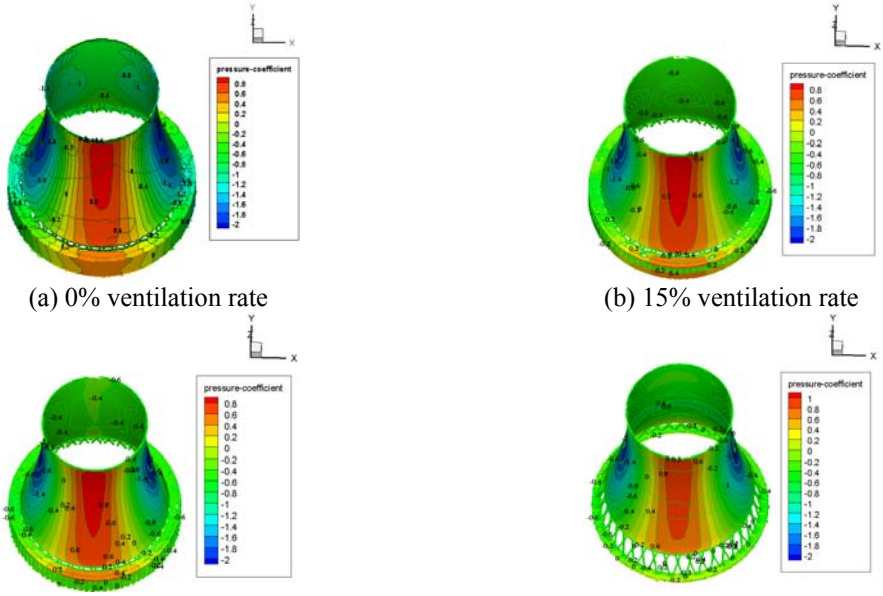

(a) 0% ventilation rate (b) 15% ventilation rate

(c) 30% ventilation rate (d) 100% ventilation rate

Fig. 10 Contours of pressure coefficient distribution on the surface of a single IDCT under different ventilation rate

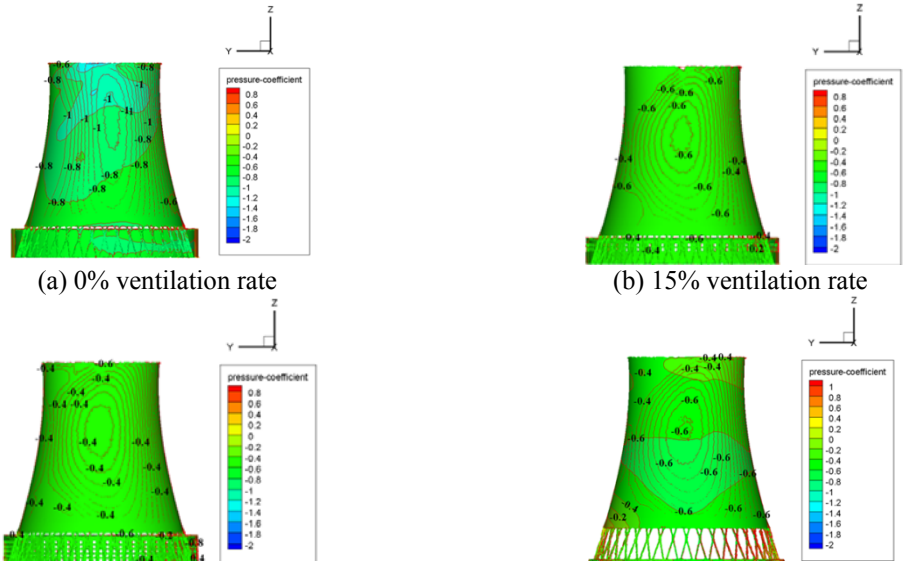

(a) 0% ventilation rate (b) 15% ventilation rate

(c) 30% ventilation rate (d) 100% ventilation rate

Fig. 11 Contours of pressure coefficient distribution on the inner surface of a single IDCT under different ventilation rate

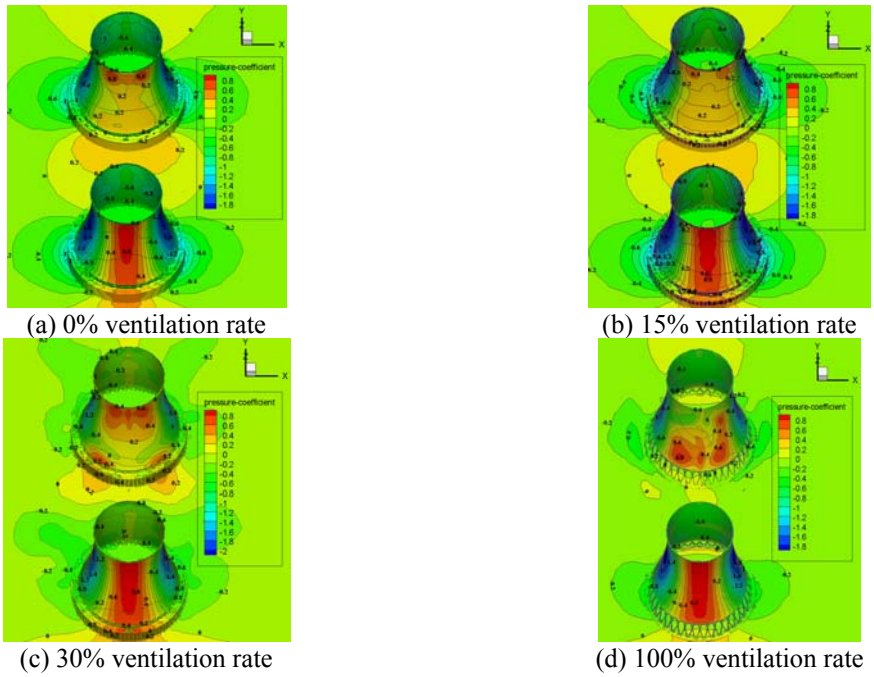

(a) 0% ventilation rate (b) 15% ventilation rate

(c) 30% ventilation rate (d) 100% ventilation rate

Fig. 12 Contours of pressure coefficient distribution on surfaces of the two-tower combination with different ventilation rates in 0° wind azimuth

4.3 Flow field investigation

The flow patterns for one and two IDCTs with different ventilation rates in 0° wind azimuth predicted by the present numerical study are shown in Figs. 13 and 14.

It is observed from Figs. 13 and 14 that the mean flow fields predicted for single IDCT with different rates are generally similar, the difference mainly lies in two aspects. One is the shape and location of vortex in the wake region, the other is the degree of the recirculating flow region contraction behind the tower models. As for the first aspect, the arch vortex for IDCT with 0% ventilation rate is at the most low location and the most flat in shape, which is in accordance with its under-prediction of global drag coefficient and the arch vortex for IDCT with 100% ventilation rate is at the most high location. As for the predication of recirculating region contraction, the contraction degree for IDCT with 0% ventilation rate is about 120 degree, which is in accordance with the results of wind tunnel test, the contraction degree for IDCT with 100% ventilation rate is most small.

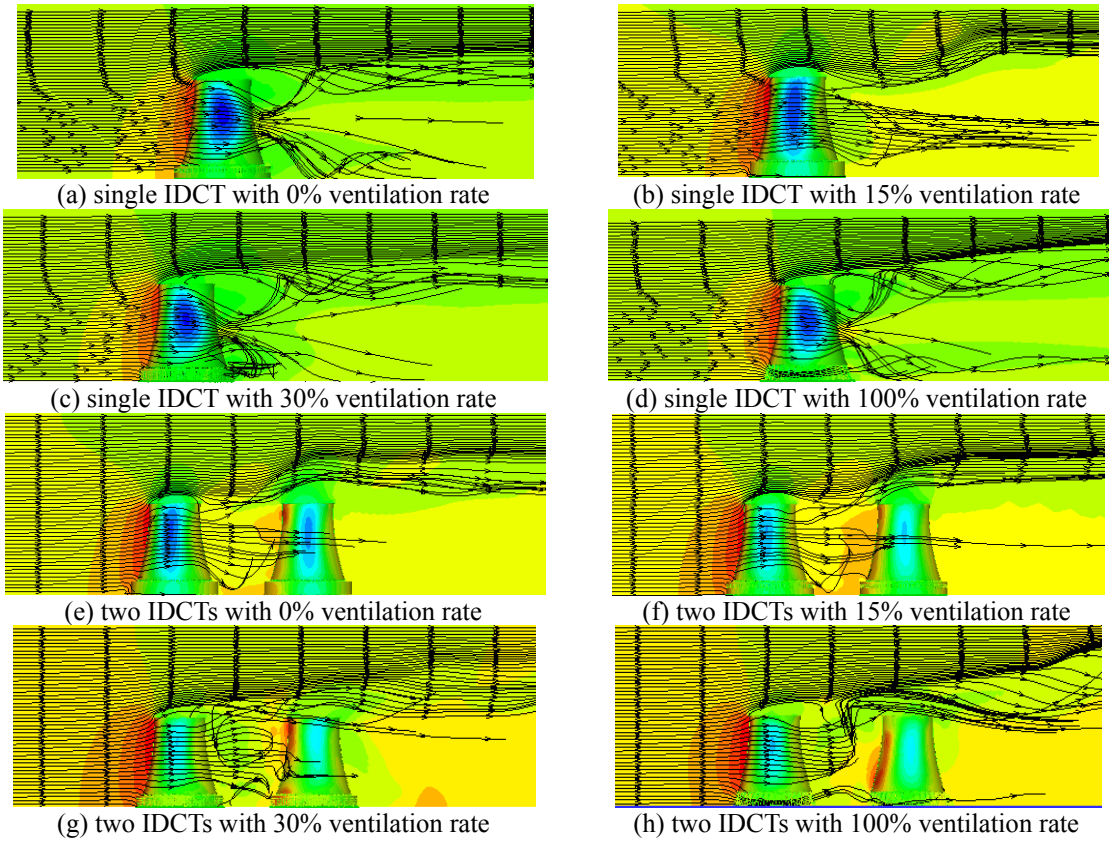

(a) single IDCT with 0% ventilation rate
(b) single IDCT with 15% ventilation rate
(c) single IDCT with 30% ventilation rate
(d) single IDCT with 100% ventilation rate
(e) two IDCTs with 0% ventilation rate
(f) two IDCTs with 15% ventilation rate
(g) two IDCTs with 30% ventilation rate
(h) two IDCTs with 100% ventilation rate

Fig. 13 Mean velocity contour distribution with different IDCT models in 0° wind azimuth

4.4 Aerodynamic interference between two towers

Fig. 15 shows the curve of the circumferential pressure coefficient distribution at 150 m altitude of the front tower in the two-tower combination with different ventilation rates in 0° wind azimuth. Comparison to the curves of circumferential pressure coefficient distribution of a single IDCT showed that the curves of the upwind and lateral surfaces (circumferential ranges of 0°-90°and 270°-360°) of the front tower with different ventilation rates were basically consistent to those of a single IDCT; however, the absolute values of the pressure coefficients on the downwind surface (circumferential range of 90°-270°) of the front tower were obviously less than the results for a single IDCT and positive pressure appeared on the downwind surface, which indicated that the influences of the interference between two towers and the ventilation rate on the distribution of the pressure coefficient on the upwind and lateral surfaces of the front towers were relatively small. However, their influences on the pressure coefficient on the downwind surface were significant. This can be explained qualitatively as that the flow which should act on the back tower was blocked and acted in the opposite direction to the downwind surface of the front tower, which caused a positive pressure to form.

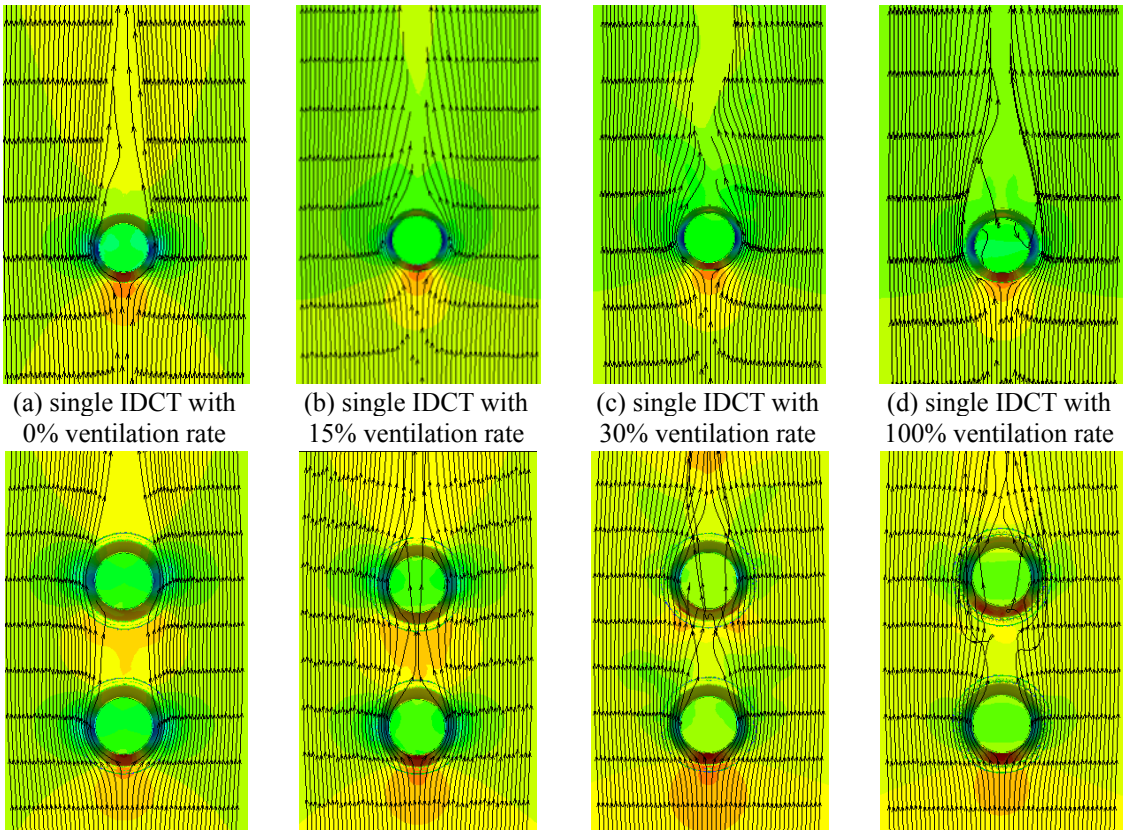

(a) single IDCT with 0% ventilation rate
(b) single IDCT with 15% ventilation rate
(c) single IDCT with 30% ventilation rate
(d) single IDCT with 100% ventilation rate
(e) two IDCTs with 0% ventilation rate
(f) two IDCTs with 15% ventilation rate
(g) two IDCTs with 30% ventilation rate
(h) two IDCTs with 100% ventilation rate

Fig. 14 Mean velocity contour distribution with different IDCT models in 0° wind azimuth

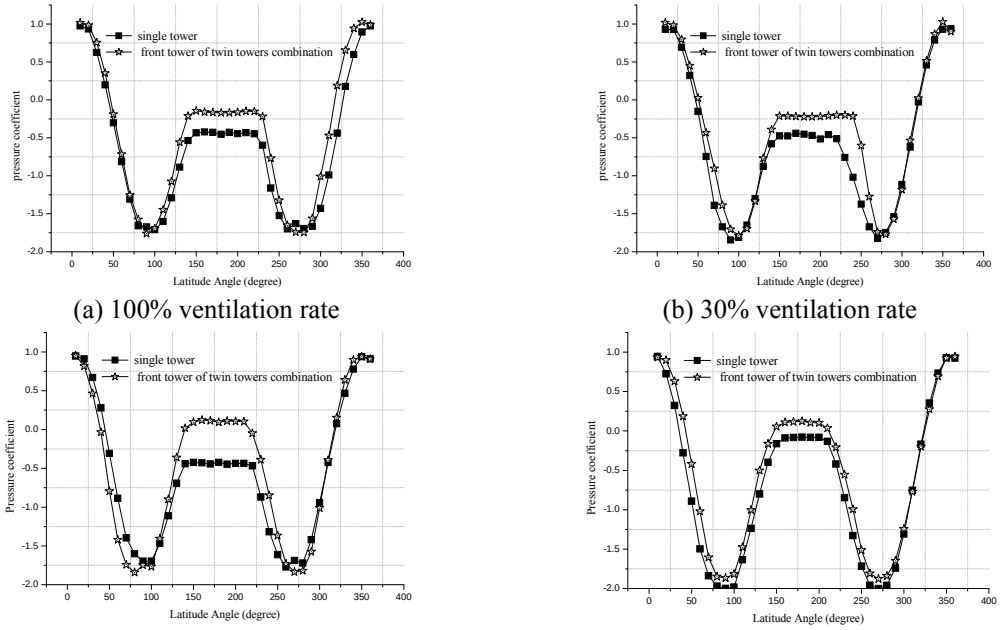

(a) 100% ventilation rate (b) 30% ventilation rate

(c) 15% ventilation rate (d) 0% ventilation rate

Fig. 15 Comparison of pressure coefficients of a single tower and the front tower in a two-tower combination with different ventilation rates in 0° wind azimuth

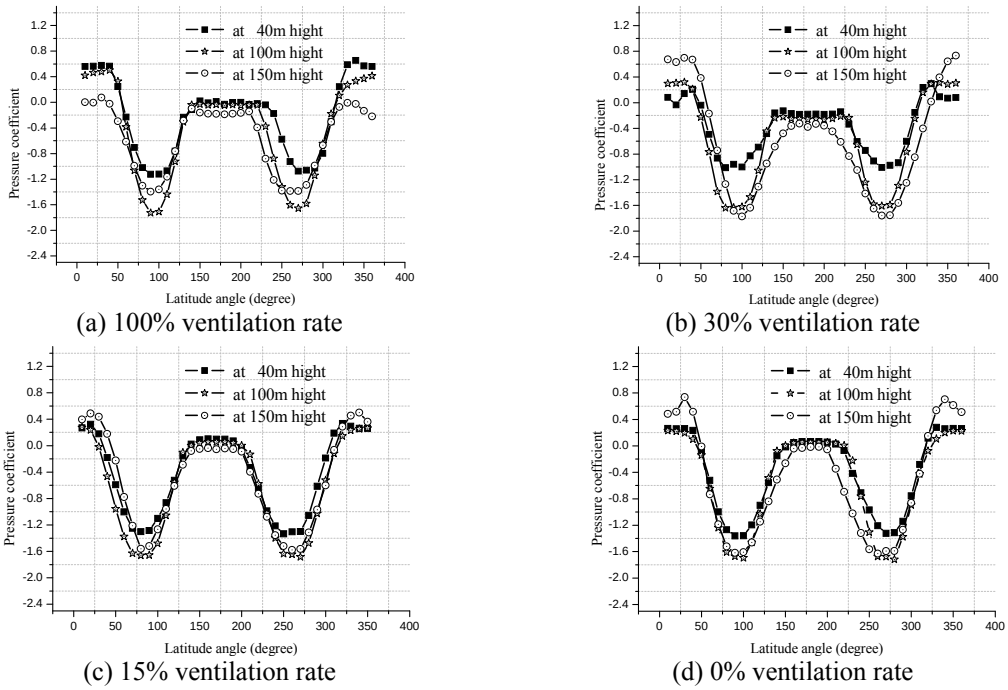

(a) 100% ventilation rate (b) 30% ventilation rate

(c) 15% ventilation rate (d) 0% ventilation rate

Fig. 16 Distributions of pressure coefficients at different altitudes of the back tower in a two-tower combination with different ventilation rates in 0° wind azimuth

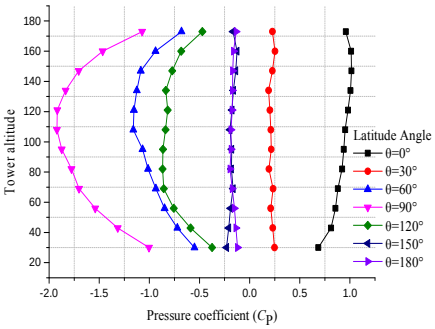

(a) 100% ventilation rate, front tower

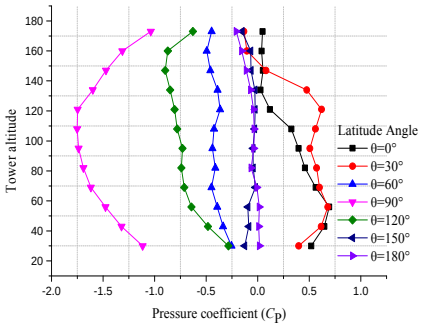

(b) 100% ventilation rate, back tower

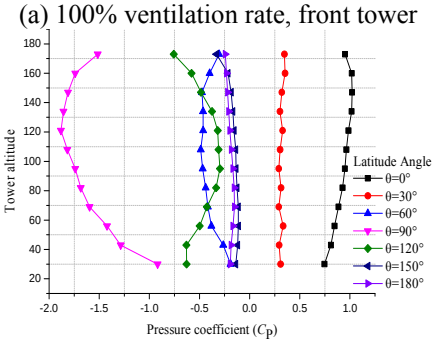

(c) 30% ventilation rate, front tower

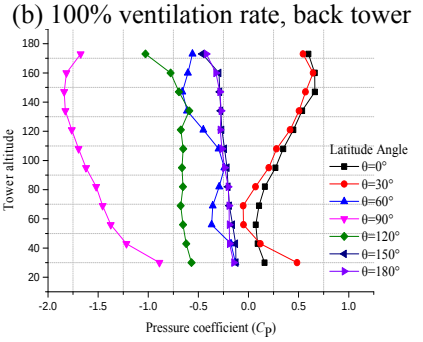

(d) 30% ventilation rate, back tower

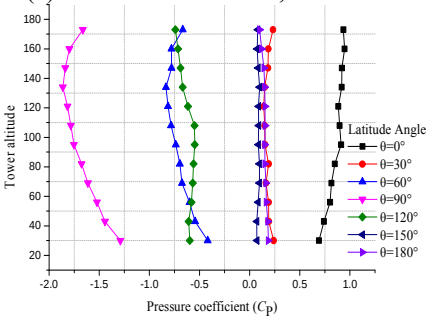

(e) 15% ventilation rate, front tower

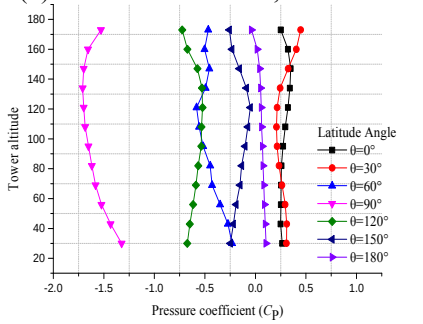

(f) 15% ventilation rate, back tower

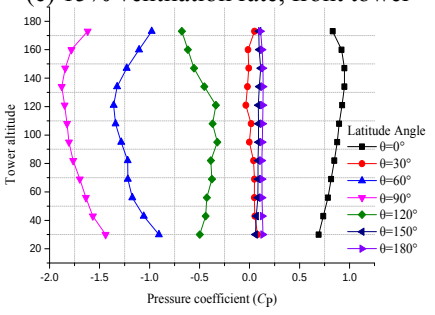

(g) 0% ventilation rate, front tower

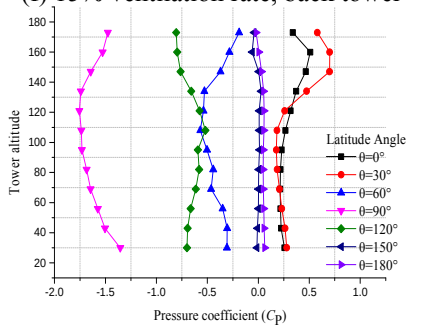

(h) 0% ventilation rate, back tower

Fig. 17 Distribution of pressure coefficients along altitude of a two-tower combination with different ventilation rates in 0° wind azimuth

Fig. 16 shows the curves of circumferential pressure coefficient distribution at 40 m, 100 m, and 150 m altitudes of the back tower in the two-tower combination with different ventilation rates in 0° wind azimuth.

It can be observed from the plots that the circumferential pressure coefficient distributions at different altitudes of the back tower in different ventilation rates are basically symmetrical. For any one ventilation rate, in the circumferential ranges of 0°-90° and 270°-360°, the pressure coefficient increased as the altitude increased. However, in the circumferential range of 180°-270°on the downwind surface, the negative pressure showed a trend of increase in magnitude as the altitude climbed. The pressure coefficients in the ranges of 0°-90° and 270°-360°at 40 m altitude of a tower with full ventilation but without a broad platform were distinguishably greater than the circumferential positive pressure values at the same altitude with other ventilation rates.

Fig. 17 illustrates the distributions of pressure coefficients along altitude at various latitude angles of the front and back towers in a two-tower combination with different ventilation rates in 0° wind azimuth. Comparison of the curves indicated that at 90° latitude angle, negative pressure coefficient reached the maximum value at the middle height and the minimum values appeared at the top and bottom of the tower. Significant wind-induced drawing forces occurred in the middle region of the tower. Positive pressure coefficients distributed approximately in the range of latitude angle of 0°-30° with different ventilation rates. The distribution of pressure coefficient along altitude on the surface of the back tower showed a trend in which the pressure decreased at the bottom and increased at the top with the increase of the ventilation rate. However, in the working condition of full ventilation, the positive pressure decreased as the altitude increased and a down-shift of the positive pressure took place. Negative pressure coefficients on the downwind surfaces in the range of latitude angle of 150°-180° of the front and back towers with different ventilation rates varied along altitude insignificantly and the negative pressure values were relatively small.

The above results demonstrate that the ventilation rate and wind azimuth significantly interfere with the wind pressure distribution on the surface of the back tower. To further explore the influence of the ventilation rate on the overall aerodynamic force on the back tower, Fig. 18 illustrates the curves of the global drag coefficients of the back tower varying with wind azimuth. Since the two towers in the combination are symmetrical by two perpendicular axes, only the drag coefficients in the range of wind azimuth 0°-90° are plotted with an increment of angle of 10°.

Fig. 18 illustrates that all the global drag coefficients of the back tower with different ventilation rates increased as the wind azimuth increased from 0° to 90°. Drag was minimized at 0° wind azimuth, which corresponds to the case in which the two towers were arranged back-and-forth along the wind direction. The drag coefficients reached the maximum at 90° wind azimuth, for which the two towers were arranged parallel to each other along the wind direction. The reason of the occurrence of the maximum drag at 90° wind azimuth may be that the back tower was out of the rear flow field of the front tower, whose eclipsing effect was reduced the most. In the range of wind azimuth 0°-30°, the slopes of curves corresponding to different ventilation rates were close to each other, indicating that in this range, the influence of the ventilation rate to the drag coefficient of the back tower was slight. For wind azimuth greater than 30°, the global drag coefficient of the back tower grew as the ventilation rate increased. The drag coefficient for full ventilation (100% ventilation rate) reached its maximum value (0.53%), which was approximately 11% greater than the maximum drag coefficient for full closure (0% ventilation rate).

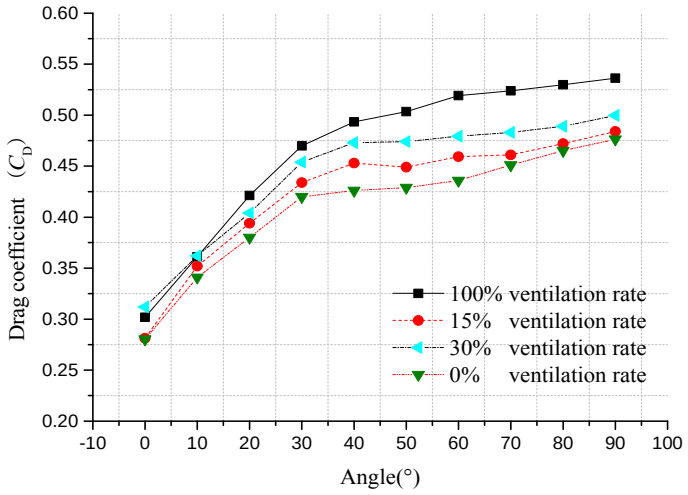

Fig. 18 Curves of the global drag coefficients of the back tower in a two-tower combination with different ventilation rates varying with the wind azimuth

5. Conclusions

Based on the CFD and wind tunnel tests, the influences of ventilation rates on the aerodynamic loads for a single IDCT or a two-tower IDCT combination during building, installation, and operation stages were revealed. Major conclusions were drawn as follows:

- The influence of the ventilation rate for a single extra-large IDCT on the pressure coefficient distribution on the outer surface was small, and the curves of mean pressure coefficients distribution were close to the reference curves provided by design norms of both China and Germany. The ventilation rate affected the internal pressure of a single IDCT, which decreased as the ventilation rate increased.
- The effects of the ventilation rates on the downwind surface of the front tower in a two-tower combination were significant. The absolute values of pressure coefficients in this region were noticeably less than those for a single tower, and positive pressure occurred. Due to the eclipsing effect of the front tower, pressure coefficients on the upwind surface of the back tower tended to be lower than those of the front tower. As the ventilation rates increased, distribution of pressure coefficients on the upwind surface of the back tower transformed from symmetrical to asymmetrical, and the region on the upwind surface of the back tower where positive pressure reached extreme values shifted gradually from the top to the bottom of the tower shell.
- In a two-tower combination, as the ventilation rate increased, the pressure coefficients distribution on the surface of the back tower along altitude showed a trend that the pressure coefficients were low at the bottom and high on the top. However, in the working condition of full ventilation, positive pressure decreased along with altitude and a down-shift of positive pressure occurred. Negative pressure coefficients on the downwind surfaces of both towers in a two-tower combination with different ventilation rates varied slightly with altitude and the negative pressure values were relatively small.

- The ventilation rate drastically influenced the global drag coefficient of the back tower in a two-tower combination. As the ventilation rate grew, the global drag coefficient of the back tower increased and reached the maximum with 100% ventilation rate (in the building stage) in 90° wind azimuth.

In summary, it was demonstrated that the aerodynamic interfering effects of the broad platform and the ventilation rate on extra-large IDCTs are significant, which are suggested to be taken into account for wind tunnel tests and wind-resistant design of such structures.

Acknowledgments

This project is jointly supported by National Natural Science Foundation (51208254 and 51021140005), Jiangsu Province Natural Science Foundation (BK2012390), and Postdoctoral Science Foundation (2013M530255; 1202006B), which are gratefully acknowledged.

References

Armitt, J. (1980), "Wind loading on cooling towers", *J. Struct. Div.*, **106**(3), 623-641.

Bartoli, G., Borri, C., Hoeffer, R. and Orlando, M. (1997), "Wind induced pressures and interference effects on a group of cooling towers in a power plant arrangement", *Proceedings of the 2nd European and African Conference on Wind Engineering*, Genoa, Italy, Padua, SGE.

Busch, D., Harte, R., Kratzig, W.B. and Montag, U. (2002), "New natural draught cooling tower of 200 mheight", *Eng. Struct.*, **24**(12), 1509-1521.

DL/T 5339-2006 (2006), *Code for hydraulic design of fossil fuel power plants*, Development and Reform Commission, P.R.C. (in Chinese)

GB/T 50102-2003 (2003), *Code for design of cooling for industrial recirculation water*, Ministry of Construction, P.R.C.(in Chinese)

Goodarzi, M. (2010), "A proposed stack configuration for dry cooling tower to improve cooling efficiency under cross wind", *J. Wind Eng. Ind. Aerod.*, **98**(12), 858-863.

Goudarzi, M. and Sabbagh-Yazdi, S. (2008). "Modeling wind ribs effects for numerical simulation external pressure load on a cooling tower of KAZERUN power plant-IRAN", *Wind Struct*., **11**(6), 479-496.

Harte, R. and Wittek, U. (2009), "Recent developments of cooling tower design", *Proceedings of the IASS Symposium*, Valencia, Spain.

Ke, S.T., Ge, Y.J., Zhao, L. and Tamura, Y. (2012), "A new methodology for analysis of equivalent static wind loads on super-large cooling towers", *J. Wind Eng. Ind. Aerod.*, **111**(3), 30-39.

Ke, S.T., Ge, Y.J., Zhao, L., Chen, S.L. and Tamura, Y. (2013), "Wind-induced responses of super-large cooling towers", *J. Central South Univ.*, **20**(11), 3216-3228.

Orlando, M. (2001), "Wind-induced interference effects on two adjacent cooling towers", *Eng. Struct.*, **23**(8), 979-992.

Jeong, S.H. (2004), "Simulation of large wind pressures by gusts on a bluff structure", *Wind Struct.*, **7**(5), 333-344.

Niemann, H.J. (1980), "Wind effects on cooling tower", *J. Struct. Div.*, **106**(3), 643-661.

Niemann, H.J. and Kopper, H.D. (1998), "Influence of adjacent buildings on wind effects on cooling towers", *Eng. Struct.*, **20**(10), 874-880.

Noh, S.Y. and Lee, S.Y. (2013), "Structural behaviour evaluation of natural draught cooling towers under the consideration of shell-geometric parameters", *Appl. Mech. Mater.*, **284**, 1396-1400.

Sun, T.F. and Gu, Z.F. (1995), "Interference between wind loading on group of structures", *J. Wind Eng. Ind.*

Aerod., **54**(55), 213-225.
Schmidt, S. and Thiele, F. (2002), "Comparison of numerical methods applied to the flow over wall-mounted cubes" , *Int. J. Heat Fluid Fl.*, **23**(3), 330- 339.
Viladkar, M.N., Karisiddappa, Bhargava, P. and Godbole, P.N. (2006), "Static soil–structure interaction response of hyperbolic cooling towers to symmetrical wind loads", *Eng. Struct.*, **28**(9), 1236-1251.
VGB-Guideline (2005), *Structural design of cooling tower- technical guideline for the structural design, computation and execution of cooling towers (VGB-R 610Ue)*, Standard Essen: BTR Bautechnikbei Kühltürmen.
Zhao, L. and Ge, Y.J. (2010), "Wind loading characteristics of super-large cooling towers", *Wind Struct*., **13**(4), 257-274.
Zhang, J.F., Chen, H., Ge, Y.J., Zhao, L. and Ke, S.T. (2014), "Effects of stiffening rings on the dynamic properties of hyperboloidal cooling towers", *Struct. Eng. Mech*., **49**(5), 619-629.

CC